Analysis of Receiver Position and Velocity Uncertainty on Passive RF Cislunar SSA Architectures

Kullen Waggoner
Air Force Institute of Technology
David Curtis
Air Force Institute of Technology

ABSTRACT

This paper explores the utilization and analysis of a cislunar-based receiver to enhance a network of terrestrial and near-earth space-based passive RF receivers for conducting Space Situational Awareness (SSA) of objects in cislunar space. It models and explores the integration of a cislunar receiver into a network of terrestrial and GEO-based receivers. The added receivers are in various periodic, closed orbits around the Earth-Moon Lagrange points L_1, L_2, and L_5. The addition of the cislunar receiver is beneficial as the estimation accuracy of passive RF systems is based on the geometric orientation of the constituent emitter and receivers and a diverse geometric setup provides greater theoretical accuracy. The orientation's usefulness for estimation is often measured through the metric of the dilution of precision (DOP). This research effort applies and adapts previous research into UAV-based passive RF estimation where receiver position and velocity uncertainty are considered and adapts/applies it to the problem of augmenting a terrestrial and near-earth passive RF architecture with a cislunar receiver. Provided is a derivation of the relationship between the receivers' position and velocity uncertainties and relates that to the Cramer-Rao Lower Bound of the anticipated final estimation accuracy of the cislunar emitter.

1. INTRODUCTION

Over the past five years, the proliferation of US, foreign, and commercial missions to and around the moon has necessitated the US to improve and prioritize spacecraft tracking and cislunar SSA capabilities [1–3]. Due to limitations in current electro-optical and radar tracking architectures for objects around the moon, there's a growing interest in novel methods for maintaining SSA. Consequently, passive RF estimation research has garnered increased attention as a means to address some of the gaps in spacecraft tracking within the cislunar regime. Multi-receiver passive RF systems measure a signal sent from a single emitter and compare the signal as it received at multiple receiver stations to calculate a time difference of arrival (TDOA) and frequency difference of arrival (FDOA). Previous research conducted at the University of Arizona demonstrated that terrestrial-based receivers can successfully track spacecraft between the Earth and the Moon using passive RF [4,5].

Recent research efforts explored the use of passive RF measurements utilizing receivers that are in near-Earth orbits or on the surface of the Earth [6–8]. However, there is interest in using future cislunar satellites for SSA and tracking throughout the cislunar region. AFRL has announced the Oracle program whose stated is "lead the development of SSA capabilities in cislunar space" and will be equipped with wide and narrow field-of-view sensors [9]. Furthermore, the exploration of further exotic orbits and locations for cislunar SSA is being evaluated in the literature [10,11]. The use of a satellite in a region of interest in space for conducting SSA is not an entirely novel idea. Currently, the USSF operates the Geosynchronous Space Situational Awareness Program (GSSAP) satellites operating near the GEO belt for the express purpose of augmenting the SSN for SSA [12]. A difficulty of using cislunar satellites for orbit determination or state estimation of other satellites is that accurate knowledge of your own satellite's state vector is an unknown. Or to articulate this problem in a different way, position, navigation, and timing (PNT) information is not readily available in the cislunar region where satellites are much farther from the GNSS satellite constellations of GPS, GLONASS, Beidou, and Galileo. This paper explores how adding a theoretical passive RF receiver to an architecture of near-Earth and terrestrial passive RF receivers improves the dilution of precision and estimation accuracy when considering position and velocity uncertainty of the receivers.

2. BACKGROUND

2.1 Cislunar PNT

Satellites operating near the Earth are able to leverage PNT services from the various GNSS satellite constellations in Earth orbit. However, this is a less reliable option for cislunar satellites. Weak GNSS, which is a method that uses the same GNSS satellites and signals as users on Earth and in near-Earth orbit utilize, provides potentially inaccurate PNT solutions [13]. When higher fidelity PNT solutions are required in cislunar space, NASA's DSN is used. This is a non-scalable solution as the network is currently near its capacity [105]. These facts have motivated research into how we should do 'GPS in cislunar'? including on where priority for coverage should be focused within the very massive region of cislunar space [106,107]. Despite the interest, conclusive efforts are still in the far future and requirements and anticipated future PNT resolution is still an open question. The best available source of PNT accuracy requirements is based on a NASA report that focuses on key navigation requirement for various mission types [108]. The document provides a requirement of 3-D positioning for cislunar type relay spacecraft between 10m and 100m for the 1-sigma accuracy.

2.2 DOP Derivation with Receiver Uncertainty Consideration

DOP is a deterministic quantity that provides an insight into how well a particular alignment of receivers will be able to provide a stochastic estimation of the emitter's state. There are multiple ways in which to derive DOP, and it is used within many research communities. The most widely used DOP is used by GNSS constellations to provide a measurement of how accurate of a PNT estimation, a user will acquire based on the location of the available satellites in-view. DOP can be accurately expressed as a relationship between the estimation error and the measurement noise. This description provides the most instinctual perception of the information that it provides. However, to incorporate receiver uncertainty, the derivation provided uses a separate starting point of using the DOP relationship to the Cramer Rao Lower Bound (CRLB). This leads to a similar result, the relationship between the states being estimated and the measurement noise, but enables the additional consideration of non-perfect receiver state knowledge. This derivation follows a similar derivation from that presented in the literature for passive RF sensing using UAVs [14,15].

The first step of this derivation is to define a vector ($\boldsymbol{\alpha}$) of $\boldsymbol{m}$ pairs of TDOA ($\boldsymbol{\Delta\tau_i}$) and FDOA ($\boldsymbol{\Delta f_i}$) measurements from the receivers with the associated measurement covariance for each measurement pair ($\boldsymbol{Q_\alpha}$).

$$\boldsymbol{\alpha} = [\Delta\tau_1 \quad \Delta f_1 \quad \Delta\tau_2 \quad \Delta f_2 \quad \dots \quad \Delta\tau_m \quad \Delta f_m]^T \tag{1}$$

$$Q_\alpha = E(\boldsymbol{\alpha}\boldsymbol{\alpha}^T) = \begin{bmatrix} \sigma_{\tau_1}^2 & 0 & 0 & 0 & 0 \\ 0 & \sigma_{\Delta f_1}^2 & 0 & 0 & 0 \\ 0 & 0 & \dots & 0 & 0 \\ 0 & 0 & 0 & \sigma_{\tau_m}^2 & 0 \\ 0 & 0 & 0 & 0 & \sigma_{\Delta f_m}^2 \end{bmatrix} \tag{2}$$

Next, we create a vector ($\boldsymbol{\beta}$) that includes all of the receiver position and velocity states as well as the covariance of the uncertainty for each receiver ($\boldsymbol{Q_\beta}$). There are $\boldsymbol{s}$ total receivers.

$$\boldsymbol{\beta} = \begin{bmatrix} \boldsymbol{X}_{r1} \\ \boldsymbol{X}_{r2} \\ \dots \\ \boldsymbol{X}_{rs} \end{bmatrix} \tag{3}$$

$$\boldsymbol{X}_{ri} = [x_i \quad y_i \quad z_i \quad v_{x_i} \quad v_{y_i} \quad v_{z_i}]^T$$

$$Q_\beta = E(\boldsymbol{\beta}\boldsymbol{\beta}^T) = \begin{bmatrix} \sigma_{r_1}^2 & 0_{6\times6} & \dots & 0_{6\times6} & 0_{6\times6} \\ 0_{6\times6} & \sigma_{r2}^2 & \dots & 0_{6\times6} & 0_{6\times6} \\ \vdots & \vdots & \ddots & \vdots & \vdots \\ 0_{6\times6} & 0_{6\times6} & \dots & \sigma_{r(s-1)}^2 & 0_{6\times6} \\ 0_{6\times6} & 0_{6\times6} & \dots & 0_{6\times6} & \sigma_{rs}^2 \end{bmatrix}$$

Where

$$\sigma_{r_i}^2 = \begin{bmatrix} \sigma_{x_i}^2 & 0 & \dots & 0 & 0 \\ 0 & \sigma_{y_i}^2 & \dots & 0 & 0 \\ \vdots & \vdots & \ddots & \vdots & \vdots \\ 0 & 0 & \dots & \sigma_{v_{y_i}}^2 & 0 \\ 0 & 0 & \dots & 0 & \sigma_{v_{z_i}}^2 \end{bmatrix} \tag{4}$$

The multivariate PDFs for each $\boldsymbol{\alpha}$ and $\boldsymbol{\beta}$, where $\boldsymbol{\alpha_0}$ and $\boldsymbol{\beta_0}$ represent the mean of each distribution [16] are:

$$f(\boldsymbol{\alpha}) = \frac{1}{2\pi^{m/2}|Q_\alpha|^{1/2}} \exp\left(-\frac{1}{2}(\boldsymbol{\alpha}-\boldsymbol{\alpha_0})^T Q_\alpha^{-1}(\boldsymbol{\alpha}-\boldsymbol{\alpha_0})\right) \tag{5}$$

$$f(\boldsymbol{\beta}) = \frac{1}{2\pi^{s/2}|Q_\beta|^{1/2}} \exp\left(-\frac{1}{2}(\boldsymbol{\beta}-\boldsymbol{\beta_0})^T Q_\beta^{-1}(\boldsymbol{\beta}-\boldsymbol{\beta_0})\right) \tag{6}$$

The next step combines the true emitter and receiver states into a single vector ($\boldsymbol{\theta}$) and the stochastic measurement and receiver states ($\boldsymbol{v}$) into a single vector.

$$\boldsymbol{\theta} = \begin{bmatrix} \boldsymbol{X}_{e_{true}} \\ \boldsymbol{\beta}_{true} \end{bmatrix} \ (true\ values)\ , \boldsymbol{v} = \begin{bmatrix} \boldsymbol{\alpha} \\ \boldsymbol{\beta} \end{bmatrix} \tag{7}$$

The derivation now begins to evaluate the CRLB as defined in Equation (8).

$$CRLB(\boldsymbol{\theta}) = -E\left[\frac{\partial^2 \ln\big(f(\boldsymbol{v}|\boldsymbol{\theta})\big)}{\partial\boldsymbol{\theta}\partial\boldsymbol{\theta}^T}\right]^{-1} \tag{8}$$

Where $\boldsymbol{\alpha}$ and $\boldsymbol{\beta}$ are independent, therefore:

$$f(\boldsymbol{v}|\boldsymbol{\theta}) = f(\boldsymbol{\alpha}|\boldsymbol{\theta}) \bullet f(\boldsymbol{\beta}|\boldsymbol{\theta}) \tag{9}$$

Using properties of the natural logarithm of the pdf simplifies the summation of the distributions into:

$$\begin{aligned} \ln\big(f(\boldsymbol{v}|\boldsymbol{\theta})\big) &= ln\big(f(\boldsymbol{\alpha}|\boldsymbol{\theta})\big) + \ln\big(f(\boldsymbol{\beta}|\boldsymbol{\theta})\big) \\ &= k_1 - \frac{1}{2}(\boldsymbol{\alpha}-\boldsymbol{\alpha_0})^T Q_\alpha^{-1}(\boldsymbol{\alpha}-\boldsymbol{\alpha_0}) + k_2 - \frac{1}{2}(\boldsymbol{\beta}-\boldsymbol{\beta_0})^T Q_\beta^{-1}(\boldsymbol{\beta}-\boldsymbol{\beta_0}) \end{aligned} \tag{10}$$

Where,

$$k_1 = \ln\left(\frac{1}{2\pi^{m/2}|Q_\alpha|^{1/2}}\right) \text{ and } k_2 = \ln\left(\frac{1}{2\pi^{s/2}|Q_\beta|^{1/2}}\right)$$

To simplify the calculations associated with the CRLB, the CRLB is subdivided into four submatrices.

$$CRLB(\boldsymbol{\theta}) = \begin{bmatrix} X_{(6\times6)} & Y_{(6\times6s)} \\ \big(Y_{(6\times6s)}\big)^T & Z_{(6s\times6s)} \end{bmatrix}^{-1} \tag{11}$$

Where $\boldsymbol{X}, \boldsymbol{Y}$, and $\boldsymbol{Z}$ are defined in the following way:

$$X = E\left[\frac{\partial^2 lnf(\boldsymbol{v}|\boldsymbol{\theta})}{\partial \boldsymbol{X}_{e_{true}} \partial \boldsymbol{X}_{e_{true}}{}^T}\right] = \left(\frac{\partial \boldsymbol{\alpha}}{\partial \boldsymbol{X}_{e_{true}}}\right)^T Q_\alpha^{-1}\left(\frac{\partial \boldsymbol{\alpha}}{\partial \boldsymbol{X}_{e_{true}}}\right) + \left(\frac{\partial \boldsymbol{\beta}}{\partial \boldsymbol{X}_{e_{true}}}\right)^T Q_\beta^{-1}\left(\frac{\partial \boldsymbol{\beta}}{\partial \boldsymbol{X}_{e_{true}}}\right)$$
$$= \left(\frac{\partial \boldsymbol{\alpha}}{\partial \boldsymbol{X}_{e_{true}}}\right)^T Q_\alpha^{-1}\left(\frac{\partial \boldsymbol{\alpha}}{\partial \boldsymbol{X}_{e_{true}}}\right) \tag{12}$$

Note: $\left(\frac{\partial \boldsymbol{\beta}}{\partial \boldsymbol{X}_{e_{true}}}\right) = 0$

$$Y = E\left[\frac{\partial^2 lnf(\boldsymbol{v}|\boldsymbol{\theta})}{\partial \boldsymbol{X}_{e_{true}} \partial \boldsymbol{\beta}_{true}^T}\right] = \left(\frac{\partial \boldsymbol{\alpha}}{\partial \boldsymbol{X}_{e_{true}}}\right)^T Q_\alpha^{-1}\left(\frac{\partial \boldsymbol{\alpha}}{\partial \boldsymbol{\beta}_{true}}\right) + \left(\frac{\partial \boldsymbol{\beta}}{\partial \boldsymbol{X}_{e_{true}}}\right)^T Q_\beta^{-1}\left(\frac{\partial \boldsymbol{\beta}}{\partial \boldsymbol{\beta}_{true}}\right)$$
$$= \left(\frac{\partial \boldsymbol{\alpha}}{\partial \boldsymbol{X}_{e_{true}}}\right)^T Q_\alpha^{-1}\left(\frac{\partial \boldsymbol{\alpha}}{\partial \boldsymbol{\beta}_{true}}\right) \tag{13}$$

$$Z = E\left[\frac{\partial^2 lnf(\boldsymbol{v}|\boldsymbol{\theta})}{\partial \boldsymbol{\beta}_{true} \partial \boldsymbol{\beta}_{true}^T}\right] = \left(\frac{\partial \boldsymbol{\alpha}}{\partial \boldsymbol{\beta}_{true}}\right)^T Q_\alpha^{-1}\left(\frac{\partial \boldsymbol{\alpha}}{\partial \boldsymbol{\beta}_{true}}\right) + \left(\frac{\partial \boldsymbol{\beta}}{\partial \boldsymbol{\beta}_{true}}\right)^T Q_\beta^{-1}\left(\frac{\partial \boldsymbol{\beta}}{\partial \boldsymbol{\beta}_{true}}\right)$$
$$= \left(\frac{\partial \boldsymbol{\alpha}}{\partial \boldsymbol{\beta}_{true}}\right)^T Q_\alpha^{-1}\left(\frac{\partial \boldsymbol{\alpha}}{\partial \boldsymbol{\beta}_{true}}\right) + Q_\beta^{-1} \tag{14}$$

Note: $\left(\frac{\partial \boldsymbol{\beta}}{\partial \boldsymbol{\beta}_{true}}\right) = I$

Now, applying the partitioned matrix inversion formula per the Shur complement [17],

$$CRLB(\boldsymbol{\theta}) = \begin{bmatrix} X & Y \\ Y^T & Z \end{bmatrix}^{-1}$$
$$= \begin{bmatrix} X^{-1} + X^{-1}Y(Z - Y^T X^{-1} Y)^{-1} Y^T X^{-1} & -X^{-1}Y(Z - Y^T X^{-1} Y)^{-1} \\ -(Z - Y^T X^{-1} Y)^{-1} Y^T X^{-1} & (Z - Y^T X^{-1} Y)^{-1} \end{bmatrix} \tag{15}$$

For this derivation, only the top left quadrant is useful for the DOP as it describes the CRLB of the emitter states.

$$CRLB(\boldsymbol{\theta})_{top\ left} = X^{-1} + X^{-1}Y(Z - Y^T X^{-1} Y)^{-1} Y^T X^{-1} \tag{16}$$

It is worthy of note, that if only the first part of the CRLB in Equation (16) is calculated, ($\boldsymbol{X^{-1}}$), then the CRLB and the subsequent DOP will be the same as if no receiver uncertainty is considered [7].

$$DOP = \frac{\sqrt{trace\left(CRLB_{(6\times6)}\right)}}{\sigma_{TDOA}} \tag{17}$$

The ***trace*** operator adds diagonal elements of the ***CRLB*** matrix together. This is problematic as the units along the diagonal are dissimilar. The top three describe uncertainty in the position states of the emitter and the bottom three describe velocity state estimation uncertainty. To maintain unit consistency, the DOP is divided into the GDOP and the VDOP where the GDOP contains the top three elements of the diagonal and the VDOP contains the next three elements.

$$GDOP = \frac{\sqrt{trace\left(CRLB_{(position)}\right)}}{\sigma_{TDOA}} \tag{18}$$

$$VDOP = \frac{\sqrt{trace\left(CRLB_{(velocity)}\right)}}{\sigma_{TDOA}} \tag{19}$$

2.2 Partial Derivative Matrices

The next step in finding the DOP is to define and derive the partial derivatives that compose the submatrices $X, Y,$ and Z from Equations (15) – (16). First the measurement equations for TDOA and FDOA must be explicitly stated. The TDOA (τ) provided in Equation (20) is directly related to the difference in the relative range between each receiver and the emitter and inversely proportional to the propagation velocity or speed of light for RF signals (c) [18,19]. $\boldsymbol{\rho_i}$ and $\boldsymbol{\rho_j}$ represent the relative position of the emitter with respect to sensors i and j. As shown in Equation (21), FDOA (Δf) is directly related to the difference in the relative radial velocity or range-rate of each receiver to the emitter [18,19]. $\boldsymbol{v_e}$ represent the emitter velocity, $\boldsymbol{v_j}$ and $\boldsymbol{v_i}$ represent the respective the sensor's velocity, and f_0 represents the signal carrier frequency.

$$G_{TDOA} = \tau = \frac{1}{c}\left[\|\boldsymbol{\rho_j}\| - \|\boldsymbol{\rho_i}\|\right] \tag{20}$$

$$G_{FDOA} = \Delta f = \frac{f_0}{c}\left(\left(\frac{\boldsymbol{\rho_j}}{\|\boldsymbol{\rho_j}\|}\right)^T(\boldsymbol{v_e} - \boldsymbol{v_j}) - \left(\frac{\boldsymbol{\rho_i}}{\|\boldsymbol{\rho_i}\|}\right)^T(\boldsymbol{v_e} - \boldsymbol{v_i})\right) \tag{21}$$

The first partial $\left(\partial\boldsymbol{\alpha}/\partial\boldsymbol{X}_{e_{true}}\right)$ is similar to the measurement Jacobians. The full partial derivative matrix which is a $2m \times 6$ sized matrix is:

$$\left(\frac{\partial\boldsymbol{\alpha}}{\partial\boldsymbol{X}_{e_{true}}}\right) = \begin{bmatrix} \frac{\partial\tau_1}{\partial x_{e_{true}}} & \frac{\partial\tau_1}{\partial y_{e_{true}}} & \frac{\partial\tau_1}{\partial z_{e_{true}}} & \frac{\partial\tau_1}{\partial v_{x_{e_{true}}}} & \frac{\partial\tau_1}{\partial v_{y_{e_{true}}}} & \frac{\partial\tau_1}{\partial v_{z_{e_{true}}}} \\ \frac{\partial\Delta f_1}{\partial x_{e_{true}}} & \frac{\partial\Delta f_1}{\partial y_{e_{true}}} & \frac{\partial\Delta f_1}{\partial z_{e_{true}}} & \frac{\partial\Delta f_1}{\partial v_{x_{e_{true}}}} & \frac{\partial\Delta f_1}{\partial v_{y_{e_{true}}}} & \frac{\partial\Delta f_1}{\partial v_{z_{e_{true}}}} \\ \vdots & \vdots & \vdots & \vdots & \vdots & \vdots \\ \frac{\partial\tau_m}{\partial x_{e_{true}}} & \frac{\partial\tau_m}{\partial y_{e_{true}}} & \frac{\partial\tau_m}{\partial z_{e_{true}}} & \frac{\partial\tau_m}{\partial v_{x_{e_{true}}}} & \frac{\partial\tau_m}{\partial v_{y_{e_{true}}}} & \frac{\partial\tau_m}{\partial v_{z_{e_{true}}}} \\ \frac{\partial\Delta f_m}{\partial x_{e_{true}}} & \frac{\partial\Delta f_m}{\partial y_{e_{true}}} & \frac{\partial\Delta f_m}{\partial z_{e_{true}}} & \frac{\partial\Delta f_m}{\partial v_{x_{e_{true}}}} & \frac{\partial\Delta f_m}{\partial v_{y_{e_{true}}}} & \frac{\partial\Delta f_m}{\partial v_{z_{e_{true}}}} \end{bmatrix} \tag{22}$$

Using the notation used in this derivation, the partial of the m^{th} sensor with respect to $x_{e_{true}}$ using receivers i and j is:

$$\frac{\partial\tau_m}{\partial x_{e_{true}}} = \left(\frac{(x_{e_{true}} - x_j)}{\rho_j} - \frac{(x_{e_{true}} - x_i)}{\rho_i}\right) \tag{23}$$

It is likewise for the remaining position partials. The velocity partial for the TDOA is zero as TDOA is not a function of velocity. For FDOA, the position partial and velocity partial for the x coordinate are:

x coordinate position partial:

$$\begin{aligned} \frac{\partial\Delta f_m}{\partial x_{e_{true}}} = \frac{f_0}{c}\Bigg(\Bigg(&\left(v_{x_{e_{true}}} - v_{xj}\right)\left(\frac{1}{\rho_j} - \frac{\left(x_{e_{true}} - x_j\right)^2}{\rho_j^3}\right) - \left(v_{y_{e_{true}}} - v_{yj}\right)\left(\frac{(x_{e_{true}} - x_j)(y_{e_{true}} - y_j)}{\rho_j^3}\right) \\ &- \left(v_{z_{e_{true}}} - v_{zj}\right)\left(\frac{(x_{e_{true}} - x_j)(z_{e_{true}} - z_j)}{\rho_j^3}\right)\Bigg) \\ &- \Bigg(\left(v_{x_{e_{true}}} - v_{xi}\right)\left(\frac{1}{\rho_1} - \frac{\left(x_{e_{true}} - x_i\right)^2}{\rho_i^3}\right) - \left(v_{y_{e_{true}}} - v_{yi}\right)\left(\frac{(x_{e_{true}} - x_i)(y_{e_{true}} - y_i)}{\rho_i^3}\right) \\ &- \left(v_{z_{e_{true}}} - v_{zi}\right)\left(\frac{(x_{e_{true}} - x_1)(z_{e_{true}} - z_1)}{\rho_i^3}\right)\Bigg)\Bigg) \end{aligned} \tag{24}$$

x coordinate velocity partial:

$$\frac{\partial\Delta f_m}{\partial v_{x_{e_{true}}}} = \frac{f_0}{c}\left(\frac{x_{e_{true}} - x_j}{\rho_j} - \frac{x_{e_{true}} - x_i}{\rho_i}\right) \tag{25}$$

The unique partial in the DOP derivation is the $(\partial \boldsymbol{\alpha}/\partial \boldsymbol{\beta}_{true})$ which in real terms is an evaluation of how the measurements change as you adjust the receiver states. For receivers labeled $1,2,\ldots s$, the partial derivative matrix for a total of s receivers become a $2m \times 6s$ sized matrix:

$$\left(\frac{\partial \alpha}{\partial \boldsymbol{\beta}_{true}}\right) = \begin{bmatrix} \frac{\partial \tau_1}{\partial x_1} & \frac{\partial \tau_1}{\partial y_1} & \frac{\partial \tau_1}{\partial z_1} & \frac{\partial \tau_1}{\partial v_{x_1}} & \frac{\partial \tau_1}{\partial v_{y_1}} & \frac{\partial \tau_1}{\partial v_{z_1}} & \cdots & \frac{\partial \tau_1}{\partial x_s} & \frac{\partial \tau_1}{\partial y_s} & \frac{\partial \tau_1}{\partial z_s} & \frac{\partial \tau_1}{\partial v_{x_s}} & \frac{\partial \tau_1}{\partial v_{y_s}} & \frac{\partial \tau_1}{\partial v_{z_s}} \\ \frac{\partial \Delta f_1}{\partial x_1} & \frac{\partial \Delta f_1}{\partial y_1} & \frac{\partial \Delta f_1}{\partial z_1} & \frac{\partial \Delta f_1}{\partial v_{x_1}} & \frac{\partial \Delta f_1}{\partial v_{y_1}} & \frac{\partial \Delta f_1}{\partial v_{z_1}} & \cdots & \frac{\partial \Delta f_1}{\partial x_s} & \frac{\partial \Delta f_1}{\partial y_s} & \frac{\partial \Delta f_1}{\partial z_s} & \frac{\partial \Delta f_1}{\partial v_{x_s}} & \frac{\partial \Delta f_1}{\partial v_{y_s}} & \frac{\partial \Delta f_1}{\partial v_{z_s}} \\ \vdots & \vdots & \vdots & \vdots & \vdots & \vdots & \ddots & \vdots & \vdots & \vdots & \vdots & \vdots & \vdots \\ \frac{\partial \tau_m}{\partial x_1} & \frac{\partial \tau_m}{\partial y_1} & \frac{\partial \tau_m}{\partial z_1} & \frac{\partial \tau_m}{\partial v_{x_1}} & \frac{\partial \tau_m}{\partial v_{y_1}} & \frac{\partial \tau_m}{\partial v_{z_1}} & \cdots & \frac{\partial \tau_m}{\partial x_s} & \frac{\partial \tau_m}{\partial y_s} & \frac{\partial \tau_m}{\partial z_s} & \frac{\partial \tau_m}{\partial v_{x_s}} & \frac{\partial \tau_m}{\partial v_{y_s}} & \frac{\partial \tau_m}{\partial v_{z_s}} \\ \frac{\partial \Delta f_m}{\partial x_1} & \frac{\partial \Delta f_m}{\partial y_1} & \frac{\partial \Delta f_m}{\partial z_1} & \frac{\partial \Delta f_m}{\partial v_{x_1}} & \frac{\partial \Delta f_m}{\partial v_{y_1}} & \frac{\partial \Delta f_m}{\partial v_{z_1}} & \cdots & \frac{\partial \Delta f_m}{\partial x_s} & \frac{\partial \Delta f_m}{\partial y_s} & \frac{\partial \Delta f_m}{\partial z_s} & \frac{\partial \Delta f_m}{\partial v_{x_s}} & \frac{\partial \Delta f_m}{\partial v_{y_s}} & \frac{\partial \Delta f_m}{\partial v_{z_s}} \end{bmatrix} \quad (26)$$

A huge portion of the matrix is zero. This is because it evaluates the change in each measurement pair with each receiver. A measurement will only be dependent on the two receivers that are used for that measurement, the primary and secondary receiver. Equation (27) restates the TDOA measurements using the equation using the i^{th} receiver as the primary and the j^{th} receiver as the secondary. The difference for all is a sign difference since the primary and secondary receivers are differenced from each other.

$$[\tau_m] = \frac{1}{c}\left[\sqrt{\left(x_{e_{true}} - x_j\right)^2 + \left(y_{e_{true}} - y_j\right)^2 + \left(z_{e_{true}} - z_j\right)^2} - \sqrt{\left(x_{e_{true}} - x_i\right)^2 + \left(y_{e_{true}} - y_i\right)^2 + \left(z_{e_{true}} - z_i\right)^2}\right] \quad (27)$$

For the m measurement, the primary (i^{th}) receiver partial becomes:

$$\begin{bmatrix} \frac{\partial \tau_m}{\partial x_i} & \frac{\partial \tau_m}{\partial y_i} & \frac{\partial \tau_m}{\partial z_i} & \frac{\partial \tau_m}{\partial v_{x_i}} & \frac{\partial \tau_m}{\partial v_{y_i}} & \frac{\partial \tau_m}{\partial v_{z_i}} \end{bmatrix} = \frac{1}{c}\begin{bmatrix} \frac{x_e - x_i}{\rho_i} & \frac{y_e - y_i}{\rho_i} & \frac{z_e - z_i}{\rho_i} & 0 & 0 & 0 \end{bmatrix} \quad (28)$$

The secondary (j^{th}) receiver partial becomes:

$$\begin{bmatrix} \frac{\partial \tau_m}{\partial x_j} & \frac{\partial \tau_m}{\partial y_j} & \frac{\partial \tau_m}{\partial z_j} & \frac{\partial \tau_m}{\partial v_j} & \frac{\partial \tau_m}{\partial v_{y_j}} & \frac{\partial \tau_m}{\partial v_{z_j}} \end{bmatrix} = \frac{1}{c}\begin{bmatrix} \frac{-(x_e - x_j)}{\rho_j} & \frac{-(y_e - y_j)}{\rho_j} & \frac{-(z_e - z_j)}{\rho_j} & 0 & 0 & 0 \end{bmatrix} \quad (29)$$

For the m measurement, the primary (i^{th}) receiver partial for the x coordinate becomes:

$$\begin{bmatrix} \frac{\partial \Delta f_m}{\partial x_i} & \frac{\partial \Delta f_m}{\partial y_i} & \frac{\partial \Delta f_m}{\partial z_i} & \frac{\partial \Delta f_m}{\partial v_{x_i}} & \frac{\partial \Delta f_m}{\partial v_{y_i}} & \frac{\partial \Delta f_m}{\partial v_{z_i}} \end{bmatrix} \quad (30)$$

x coordinate position partial: (31)

$$\frac{\partial \Delta f_m}{\partial x_i} = \frac{f_0}{c}\left(\left(v_{x_{e_{true}}} - v_{xi}\right)\left(\frac{1}{\rho_1} - \frac{\left(x_{e_{true}} - x_i\right)^2}{\rho_i^3}\right) - \left(v_{y_{e_{true}}} - v_{yi}\right)\left(\frac{\left(x_{e_{true}} - x_i\right)\left(y_{e_{true}} - y_i\right)}{\rho_i^3}\right) - \left(v_{z_{e_{true}}} - v_{zi}\right)\left(\frac{\left(x_{e_{true}} - x_i\right)\left(z_{e_{true}} - z_i\right)}{\rho_i^3}\right)\right)$$

x coordinate velocity partial:

$$\frac{\partial \Delta f_m}{\partial v_{x_i}} = \frac{f_0}{c}\left(\frac{x_e - x_i}{\rho_i}\right) \tag{32}$$

The remaining position and velocity coordinate partials are similar by symmetry.
The secondary (j^{th}) receiver partial becomes:

$$\left[\frac{\partial \Delta f_m}{\partial x_j} \quad \frac{\partial \Delta f_m}{\partial y_j} \quad \frac{\partial \Delta f_m}{\partial z_j} \quad \frac{\partial \Delta f_m}{\partial v_{x_j}} \quad \frac{\partial \Delta f_m}{\partial v_{y_j}} \quad \frac{\partial \Delta f_m}{\partial v_{z_j}}\right] \tag{33}$$

x coordinate position partial:

$$\frac{\partial \Delta f_m}{\partial x_j} = \frac{-f_0}{c}\left(\left(v_{x_{e_{true}}} - v_{xj}\right)\left(\frac{1}{\rho_1} - \frac{\left(x_{e_{true}} - x_j\right)^2}{\rho_j^3}\right) - \left(v_{y_{e_{true}}} - v_{yi}\right)\left(\frac{\left(x_{e_{true}} - x_j\right)\left(y_{e_{true}} - y_j\right)}{\rho_j^3}\right) - \left(v_{z_{e_{true}}} - v_{zj}\right)\left(\frac{\left(x_{e_{true}} - x_j\right)\left(z_{e_{true}} - z_j\right)}{\rho_j^3}\right)\right) \tag{34}$$

x coordinate velocity partial:

$$\frac{\partial \Delta f_m}{\partial v_{x_j}} = \frac{-f_0}{c}\left(\frac{x_e - x_j}{\rho_j}\right) \tag{35}$$

In summary, the above full derivation showed the calculation of the DOP for passive RF when receiver uncertainty is taken into consideration. The DOP is calculated using the trace of the CRLB (Equation (18) or (19)). The CRLB is calculated using submatrix operations as shown in Equation (16). Finally, each of the submatrices X, Y, and Z are calculated using the measurement and receiver uncertainties, Q_α and Q_β, respectively and the indexed partial derivative matrices shown in Equation (22) and Equation (26).

3. RESULTS AND DISCUSSION

3.1 Individual Cislunar Receiver Uncertainty

The simulations used closed Lagrange point or distant retrograde (DRO) cislunar orbits for the cislunar emitter and receivers. Additionally, each scenario was organized and setup in a manner similar to the one shown in Fig. 2. The first simulation shows a 21-day scenario demonstrating how DOP changes throughout a full period of a DRO emitter. For this scenario, a receiver in an L_1 halo closed orbit is added to a passive architecture that is found to perform well in previous research [7].

A major consideration not modeled in this research is the beamwidth of the transmitted signal from the emitter. For a passive RF receiver to successfully calculate a TDOA and FDOA, both receivers must be in either the main lobe or in some cases a side lobe [20]. The beamwidth size and shape are highly dependent on the transmitter characteristics used as well as the carrier frequency, and these dependencies are outside the scope of this research effort [21]. Additionally, throughout the formulation of the DOP with uncertainty, an inherent assumption of full LOS between

all receivers and the emitter is made to enable a direct comparison between architectures with and without a cislunar receiver.

Table 1. Uncertainty values for position and velocity used for scenario.

	Position Uncertainty (σ_{pos})	**Velocity Uncertainty (σ_{vel})**
Terrestrial Receivers	1 cm	1 mm/s
Near-Earth Space Receivers	1 m	.1 m/s
Cislunar Receiver	100 m*	10 m/s*

***These values varied in section 3.2 and 3.3**

The receiver architecture chosen for this scenario are six terrestrials with a single GEO as described in analysis. The geographical location of the terrestrial receivers is shown in Fig. ***1***. The setup showing the orbit of the near-Earth receiver, cislunar receiver, and the cislunar DRO emitter as well as indicating arrows shown the initial direction of travel are shown in Fig. 2.

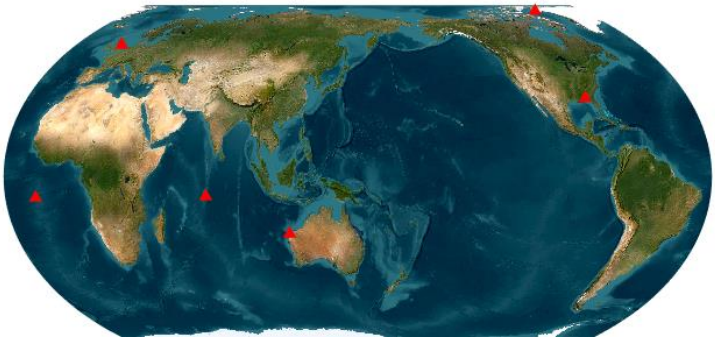

Fig. 1. Location of terrestrial receivers used for analysis are shown by red triangles.

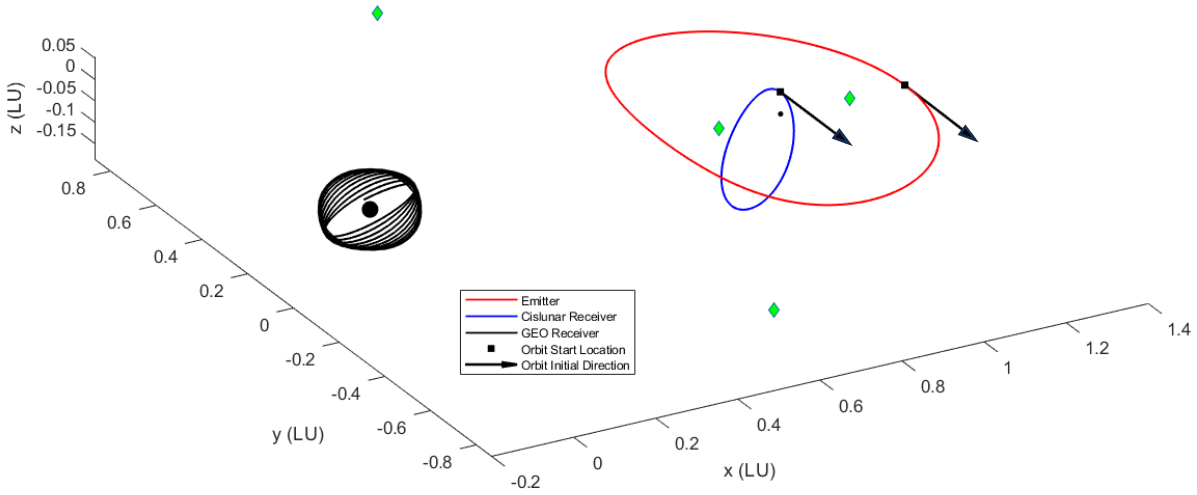

Fig. 2. Synodic frame diagram of scenario setup showing emitter in 21-day period DRO, the cislunar receiver in an L1 halo orbit and the GEO receiver in an orbit on the Earth's GEO belt. The Earth and Moon are shown in their respective locations.

The DOP varied throughout the scenario. Line of sight was considered in this scenario and only receivers that did have a clear line of sight to the emitter were used in the calculation of the DOP. A plot showing how DOP varied throughout the scenario is provided in Fig. *3* as well as the summary statistics in Table *2*. Overall, the DOP shows a U shape trend. The minimum corresponds to the halfway point of the scenario when the emitter is closest to the Earth. This is understandable because as the emitter gets closer to the Earth, there is potentially greater geometric separation

in the receiver locations. Additionally, shown on the plot is the GDOP throughout the scenario if no uncertainty is considered. The added uncertainty of the receiver positions increases the DOP, indicating worse potential estimation accuracy.

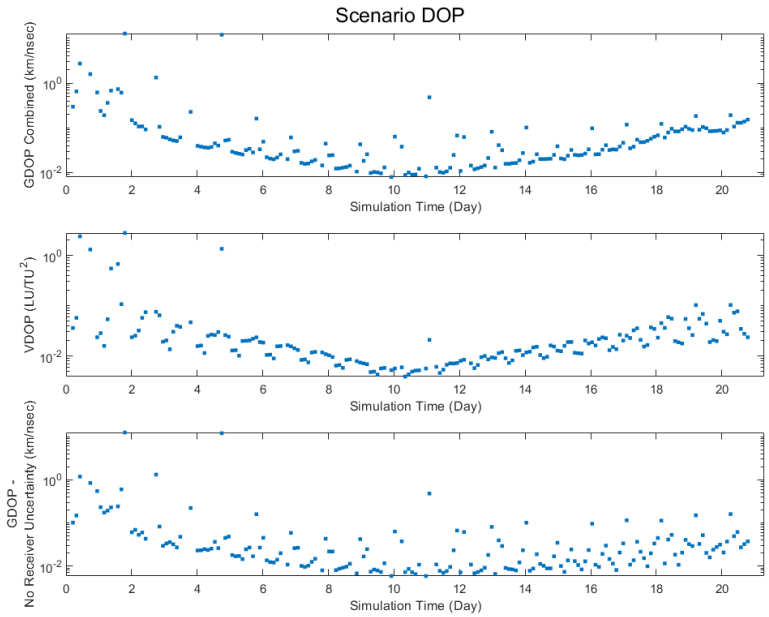

Fig. 3. DOP throughout simulation using a DRO emitter, with receivers at L1 halo, GEO, and six terrestrial based locations.

Table 2. Summary statistics of DOP scenario accounting for receiver state uncertainty

	Median	**Mean**	**Min**	**Max**
GDOP (km/nsec)	0.0353	0.2417	0.0079	12.7817
VDOP (LU/TU^2)	0.0158	0.0717	0.0039	2.7883
GDOP without receiver uncertainty (km/nsec)	0.0216	0.1992	0.0059	12.4774

3.2 GDOP Relationship with Position Uncertainty

Further analysis was conducted to explore the potential benefits of a cislunar receiver augmenting an architecture of terrestrial and near-Earth receivers. Scenarios similar to the one discussed in the previous section were run across a range of cislunar receiver uncertainties of $\mathbf{10^{-5}}\ \boldsymbol{km}$ to $\mathbf{10^{4}}\ \boldsymbol{km}$ to discover what accuracy of cislunar receiver position accuracy is predicted to be needed to improve estimation accuracy. Fig. 4-Fig. 5 show the results for the median GDOP of various cislunar receivers across $\boldsymbol{L_1}$, $\boldsymbol{L_2}$, and $\boldsymbol{L_4}$. All are conducted with the addition of six terrestrial and one GEO receiver and the target emitter in all cases is a 21-day DRO. The results from all are similar in that there is an S curve with a lower asymptote corresponding to median GDOP without the consideration of receiver uncertainty and an upper horizontal asymptote that corresponds to the median GDOP of the scenario if no cislunar receiver is present.

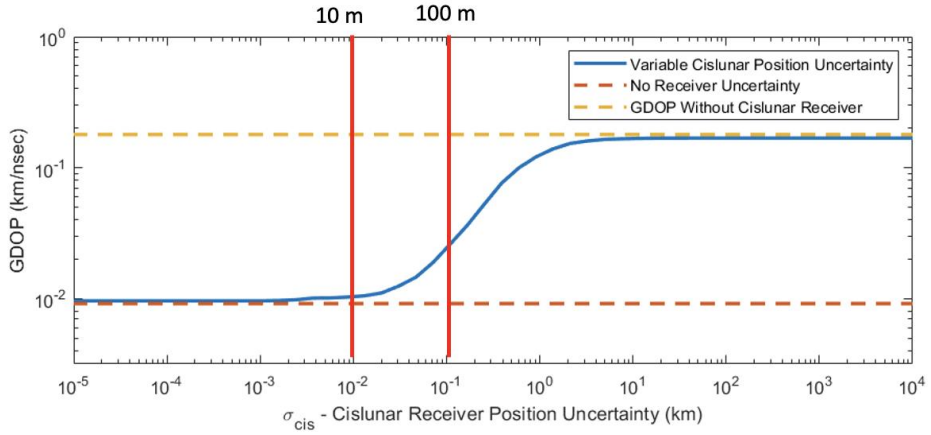

Fig. 4. Position uncertainty plots showing median scenario GDOP for TDOA and FDOA estimation varying as the cislunar receiver uncertainty varies. Cislunar receiver for this plot is an L1 halo orbiter. The red vertical lines depict potential 1-σ NASA requirements for cislunar relay spacecraft position accuracy [22].

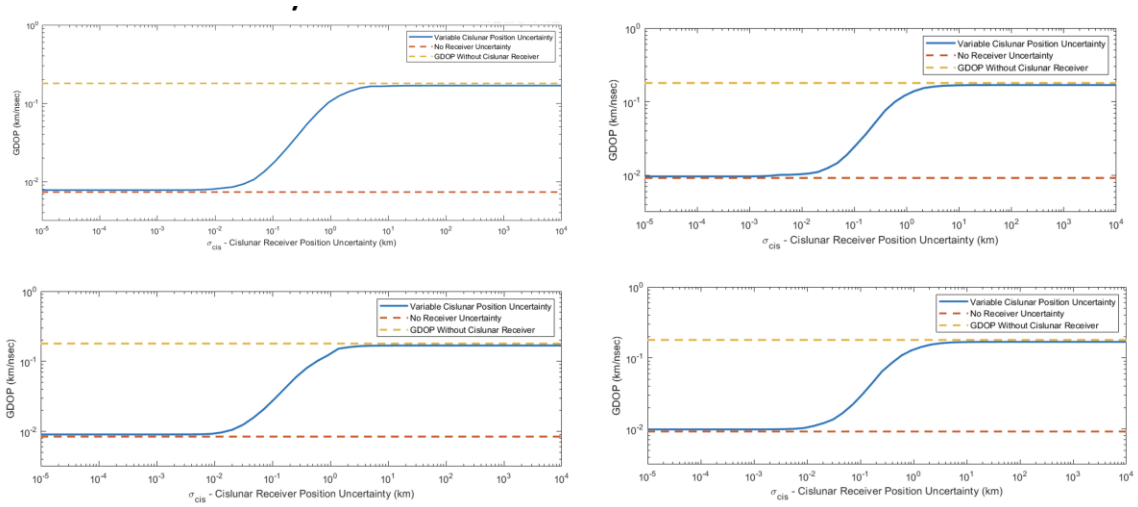

Fig. 5. Position uncertainty plots showing median scenario GDOP for TDOA and FDOA estimation varying as the cislunar receiver uncertainty varies. Top left shows an L2 NRHO receiver, top right an L1 halo receiver, bottom left an L4 planar receiver, and bottom right shows an L1 planar receiver.

The plot shows that accuracy improvements after uncertainty is $\mathbf{10^{-2}}\ \boldsymbol{km}$ or $\mathbf{10}\ \boldsymbol{m}$ is marginal and that if the position accuracy of the receiver is larger than $\mathbf{10^{0}}\ \boldsymbol{km}$ or $\mathbf{1000}\ \boldsymbol{m}$, then the cislunar receiver is predicted to provide very little benefit. It is of note that NASA requirements documents have discussed potential position uncertainty requirement ranging between $\mathbf{10}\ \boldsymbol{m}$ and $\mathbf{100}\ \boldsymbol{m}$ [22]. Finally, the addition of a cislunar receiver shows the potential to improve the predicted GDOP by over an order of magnitude over an architecture composed entirely of terrestrial and near-Earth orbiting receivers.

3.3 GDOP and VDOP Relationship with Position and Velocity Uncertainty

The relationship between the DOP and position/velocity uncertainty was further explored by varying both the position and velocity uncertainties to determine velocity uncertainty. This demonstrated a significant effect on the predicted GDOP or VDOP of the scenario. Fig. 6 and Fig. 7 show the results from simulations with varying uncertainties.

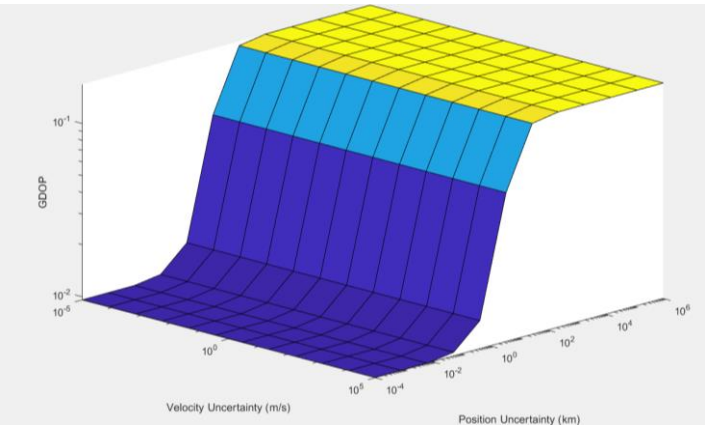

Fig. 6. Plot showing median scenario GDOP for a DRO emitter and a receiver architecture of an L1 halo, GEO, and six terrestrial nodes. GDOP is only affected by position uncertainty and not velocity uncertainty for the cislunar receiver. The units for GDOP are in km/nsec.

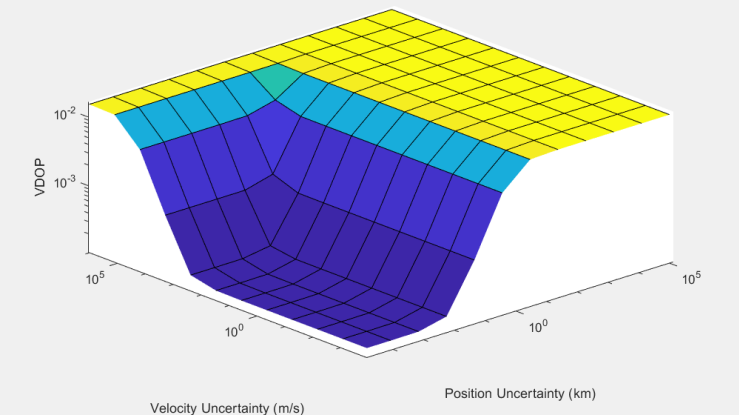

Fig. 7. Plot showing median scenario VDOP for a DRO emitter and a receiver architecture of an L1 halo, GEO, and six terrestrial nodes. VDOP is affected by both position and velocity uncertainty for the cislunar receiver. The units for VDOP are in non-dimensional CR3BP LU/TU^2.

Demonstrated in the above plots is the significant dependence on the position uncertainty of the GDOP and VDOP. The absence of a meaningful relationship between the GDOP and velocity is not surprising as the TDOA measurement is not dependent on the receiver velocity states but only the position states. The VDOP is a function of the velocity uncertainty. From Fig. *7*, it shows that when cislunar receiver's uncertainty exceeds around 100 m/s, the predicted VDOP of the architectures increases significantly.

4. SUMMARY

This paper adapted and demonstrated the derivation of a DOP metric that considers observer uncertainty and applied the DOP to passive RF estimation using cislunar receivers showing that the addition of a cislunar receiver can improve the median scenario DOP by over an order of magnitude as compared to a terrestrial/single GEO passive RF architecture. Additionally, it showed that the improvement in DOP is highly dependent on the receiver's position uncertainty and the improvement in DOP drops off significantly when position uncertainty for a cislunar receiver is greater than $10m$ (1σ). Various scenarios were constructed and modeled demonstrating the potential usefulness of the receiver-uncertain DOP in evaluating potential future cislunar SSA architectures as well as establishing future requirements for PNT systems in covering cislunar satellites. Similar to the DOP metrics in previous literature[7], this DOP allows for the calculation of a deterministic value to evaluate and compare various emitter/receiver setups to one another.

5. REFERENCES

[1] "United States Space Priorities Framework," *The White House*, 2021. Retrieved 5 August 2024. https://www.whitehouse.gov/wp-content/uploads/2021/12/United-States-Space-Priorities-Framework-_-December-1-2021.pdf

[2] "National Cislunar Science and Technology Strategy," *Cislunar Technology Strategy Interagency Working Group*, 2022. http://www.whitehouse.gov/ostp.http://www.whitehouse.gov/ostp/nstc.

[3] "SPD 3-100 Space Domain Awareness, Doctrine for Space Forces," STARCOM Delta 10, 2023.

[4] Furfaro, R., Reddy, V., Campbell, T., and Gray, B., "Tracking Objects in Cislunar Space : The Chang'e 5 Case," *Advanced Maui Optical and Space Surveillance Technologies Conference (AMOS)*, 2021, pp. 1–7.

[5] Joyce, T., Phipps, R., Jacobson, C., Battle, A., Estévez, D., Furfaro, R., and Reddy, V., "Passive RF Observations of Cislunar Objects," *Advanced Maui Optical and Space Surveillance Technologies Conference*, 2023. www.amostech.com

[6] Waggoner, K., Curtis, D. H., and Little, B., "Analysis of TDOA/FDOA State Estimation Accuracy of Cislunar Objects for Space Situational Awareness," *IEEE Aerospace Conference*, 2023.

[7] Waggoner, K. W., and Curtis, D. H., "State Estimation of Terrestrial and Space Based Passive RF Architectures for Use in Cislunar SSA Utilizing Existing SSN Locations," *Advanced Maui Optical Space Surveillance Technologies Conference*, 2023. www.amostech.com

[8] Waggoner, K. W., Curtis, D. H., and Lovell, T. A., "Cislunar Orbit Determination Using Multi-Receiver Doppler Ratios," *AIAA SCITECH 2024 Forum*, 2024.

[9] Conner, F., "AFRL's Oracle Family of Systems Developing Nation's 1st Cislunar Space Situational Awareness Capabilities," AFRL News Article. Retrieved 20 June 2024. https://www.afrl.af.mil/News/Article-Display/Article/3611977/afrls-oracle-family-of-systems-developing-nations-1st-cislunar-space-situationa/

[10] Ewart, R. M., Plotke, E., and Lai, P. C., "Pole-Sitter Based Space Domain Awareness for Cislunar Objects," *Journal of the Astronautical Sciences*, Vol. 71, No. 2, 2024. https://doi.org/10.1007/s40295-024-00430-1

[11] Dahlke, J., Wilmer, A., and Bettinger, R., "Preliminary Comparative Assessment of L2 and L3 Surveillance Using Select Cislunar Periodic Orbits Cislunar Periodic Orbits for Space Domain Awareness View Project," *AAS 22-640*, 2022. https://www.researchgate.net/publication/363383268

[12] USSF Fact Sheets, "Geosynchronous Space Situational Awareness Program." Retrieved 20 June 2024. https://www.spaceforce.mil/About-Us/Fact-Sheets/Article/2197772/geosynchronous-space-situational-awareness-program/

[13] Delépaut, A., Giordano, P., Ventura-Traveset, J., Blonski, D., Schönfeldt, M., Schoonejans, P., Aziz, S., and Walker, R., "Use of GNSS for Lunar Missions and Plans for Lunar In-Orbit Development," *Advances in Space Research*, Vol. 66, No. 12, 2020, pp. 2739–2756. https://doi.org/10.1016/j.asr.2020.05.018

[14] Ho, K. C., Lu, X., and Kovavisaruch, L., "Source Localization Using TDOA and FDOA Measurements in the Presence of Receiver Location Errors: Analysis and Solution," *IEEE Transactions on Signal Processing*, Vol. 55, No. 2, 2007, pp. 684–696. https://doi.org/10.1109/TSP.2006.885744

[15] Sun, S., Wang, Z., and Wang, Z., "Study on Optimal Station Distribution Based on TDOA Measurements," *International Conference on Computer Engineering, Information Science & Application Technology*, 2016.

[16] Tsun, A., "Chapter 5. Multiple Random Variables 5.9: The Multivariate Normal Distribution." Retrieved 20 June 2024. https://web.stanford.edu/class/archive/cs/cs109/cs109.1218/files/student_drive/5.9.pdf

[17] Zhang, F., "The Schur Complement and Its Applications," Springer, New York, NY, 2005.

[18] Mušicki, D., and Koch, W., "Geolocation Using TDOA and FDOA Measurements," *Proceedings of the 11th International Conference on Information Fusion, FUSION 2008*, 2008.

[19] Guo, F., Fan, Y., Zhou, Y., Xhou, C., and Li, Q., "Space Electronic Reconnaissance: Localization Theories and Methods," *Space Electronic Reconnaissance: Localization Theories and Methods*, 2014, pp. 1–357. https://doi.org/10.1002/9781118542200

[20] Wang, Z., Hu, D., Huang, J., Xie, M., and Zhao, C., "Optimal Station Placement Method for Three-Station TDOA Localization Under Signal Beam Constraint," *Wireless Personal Communications*, Vol. 133, No. 1, 2023, pp. 119–149. https://doi.org/10.1007/s11277-023-10754-0

[21] Larson, W., and Wertz, J., "Space Mission Analysis and Design," Springer, New York, 1999.

[22] Nelson, R. A., Brodsky, B., Oria, A. J., Connolly, J. W., Sands, O. S., Welch, B. W., Orr, R., Schuchman, L., and Rockville, M., "Key Issues for Navigation and Time Dissemination in NASA's Space Exploration Program," *NASA/TM—2006-214425*, 2006. http://www.sti.nasa.gov